

Investigation of bubble behaviour in a gas-solid fluidized bed by means of a twin-plane ECT sensor

Xiaoxu Li, Artur J. Jaworski, Xiaolan Mao

Faculty of Engineering, University of Leeds, Woodhouse Lane, Leeds, LS2 9JT, UK
cnxl@leeds.ac.uk, a.j.jaworski@leeds.ac.uk

ABSTRACT

Fluidized beds are used extensively in chemical engineering applications, such as food processing, combustion, gasification processes and pharmaceutical industry. However, due to their complex fluid mechanical characteristics (for example bubble size and bubble velocity), conventional measuring techniques do not permit a sufficient understanding. Electrical Capacitance Tomography (ECT) has been developed over the last few decades as a non-invasive measurement technique and applied to study gas-solids fluidized beds. Although many researchers investigated relationships governing bubble sizes, the influence of cut-off value (a grey level value distinguishing gas and solid phases) of bubble boundary on the bubble size estimation is still not fully understood.

A twin-plane ECT sensor with 10 mm-long measuring electrodes has been designed and fabricated to study the single bubbling regime in a gas-solids model fluidized bed. To investigate the influence of the cut-off value on bubble size estimation, different diameter hollow plastic balls have been imaged while the bed is at packed bed state. Appropriate MATLAB code has been developed to extract the cut-off values of the boundary for these plastic balls. Based on the cut-off values, bubble size within single bubbling regime has been estimated by LBP and iterative LBP image reconstruction algorithms.

Finally, estimated bubble size has been compared and analysed with existing bubble size estimation correlations. Future work will focus on the effect of different reconstruction algorithms and permittivity models on bubble size estimation to get more comprehensive understanding of bubble behaviour to examine the capability of ECT at estimating single bubble size within fluidized bed.

Keywords Bubble size estimation, COMSOL simulation, Cut-off value, ECT sensor.

1 INTRODUCTION

Over the last few decades, gas-solids fluidized beds have been applied extensively to the industrial applications, with examples of chemical engineering, power station combustion, drying and coating technology (Cheremisinoff, 1986, Dyakowski and Jaworski, 2001). Their widespread usage is attributed to their excellent heat and mass transfer rates between gas and solid phases. However, the complex nature of the hydrodynamic characteristics inside of the fluidized beds is still not fully understood. The appearance of bubbles is regarded as one of the most important inherent hydrodynamic features. Therefore, numerous traditional measuring instruments, such as capacitance, fibre optic and pressure probes, which are inserted into the fluidized beds, have been used by previous researchers to investigate the bubble behaviour. However, such invasive probes inevitably disrupt the internal flow. Therefore non-invasive methods, as discussed below, have been developed to study the hydrodynamics of the fluidized bed.

X-ray techniques have been used (Rowe, 1976) to predict the bubble size in a gas fluidized bed. High Speed Camera (HSC) was applied (Kage et al., 2000) to observe the bursting bubbles at the surface of the fluidized bed. However, the above non-invasive methods have their shortcomings. X-ray is too costly and space demanding technique and it requires a priori knowledge and skills to operate. Meanwhile, HSC can only detect bubbles bursting at the bed surface without the capability of observing the bubbles appearing in the internal bed. Compared with the above non-invasive measuring techniques, Electrical Capacitance Tomography (ECT) has been developed as a relatively

inexpensive and easy to handle non-invasive measuring instrument to investigate the gas-solid fluidized beds (Dyakowski et al., 2000).

ECT has been used by many previous researchers to attempt to estimate the bubble size, which is a very crucial parameter in depicting bubble behaviour in fluidized state. In the very early stage, Halow has observed the bubble coalescence using capacitance imaging, giving a voidage contour value (average cross-sectional emulsion phase voidage) between 0.7 to 0.75 (Halow and Nicoletti, 1992). However, the bubble sizes have not been confirmed with empirical correlations yet. Wang has estimated bubble sizes in fluidized beds and compared with correlations but, how the bubble sizes were determined – in particular the bubble boundary defined as a “cut-off” grey level value distinguishing gas and solid phases – is not clear (Wang, 1998). The effect of different permittivity models on phantom boundary estimation has been analysed by Pugsley without any further substantial investigation relating to bubbles size estimation in fluidized beds (McKeen and Pugsley, 2002). In addition, three arbitrary bubble size boundary values (0.4, 0.5 and 0.6) were used (Chandrasekera et al., 2015) to estimate bubble sizes in single bubbling fluidized beds. It is evident that, no systematic study on bubble size estimation, especially cut-off value determination, has yet been performed.

This paper is aimed at investigating the bubble sizes in a single bubbling fluidized bed by means of a 10 mm-long twin-plane ECT sensor. Firstly, five different plastic balls were imaged in a packed bed to extract the cut-off values for bubble boundaries. The plastic balls were placed near the centre and near the wall, respectively. Then, the wall effects of the real plastic balls were studied by COMSOL numerical simulation. Finally, bubble sizes were estimated based on LBP and iterative LBP image reconstruction algorithms and the results compared with widely accepted empirical correlations.

2 EXPERIMENTAL

The overall experimental rig is depicted in Fig. 1. The fluidized bed consists of 1 m long acrylic pipe with 59 mm internal diameter and 3 mm wall thickness. 48 holes of 1 mm diameter are drilled in a perforated PVC distributor. The total area of the holes in the distributor is $3.768 \times 10^{-5} \text{ m}^2$ (1.38% of the total effective area). Air for fluidization is provided by a compressed air cylinder. A needle valve acts as the isolation valve and controls the air flowing into fluidized bed. A customized cap in which a piece of fine mesh is embedded is mounted on top of the pipe to prevent the solids blowing out from the top. A float type flow meter is used to measure superficial air velocity. The static height of the fluidized bed is kept at 170 mm, which ensures that the granular material completely covers the electrodes (including guard electrodes). This is to keep the electrostatic field as two-dimensional as possible for the calibration. Silica sand is used as granular material. The density of silica sand is 2650 kg/m³, and its mean diameter is 295 microns, which satisfies the Geldard classification of Group B particles for fluidization. Its size distribution and cumulative curves can be found in Fig. 2, which is obtained by Mastersizer2000 particle size distribution analysis. A U-shaped water manometer is connected in the gas supply line to measure the pressure drop.

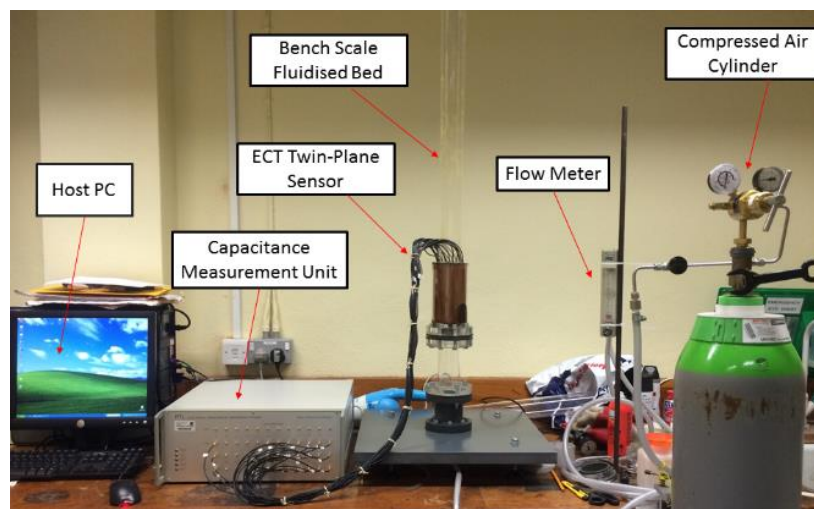


Figure 1. Overall experimental rig.

In this experiment, the PTL300E ECT system constructed by Process Tomography Ltd (UK) is used. The customized ECT sensor is connected to the data acquisition module (DAM200) and a host PC, which can also be found in Fig. 1. The detailed information of the customized ECT sensor is provided in Fig. 3.

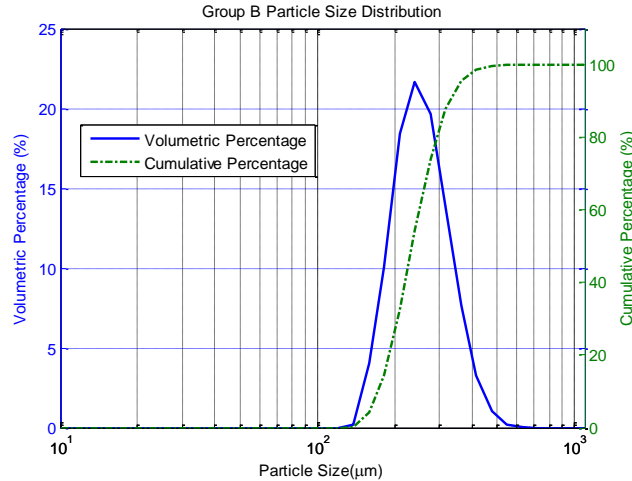


Figure 2. Particle size distribution.

The customized sensor is a twin-plane ECT sensor, with eight measuring electrodes per plane, etched on a PCB sheet. The electrode length was chosen as 10 mm as a trade-off between inter-electrode capacitance values and anticipated bubble sizes. As depicted in the left hand side figure in Fig.3, the eight measuring electrodes are placed peripherally by the external side of the fluidized bed pipe. Three sections of driven guard electrodes are mounted circumferentially between the two planes of measuring electrodes in order to prevent the electric field from being diverted to earth at the ends of the measurement electrodes, which can be seen in the right hand figure in Fig.3.

The centre-to-centre distance between the two sensor planes is 40 mm, which was designed as a trade-off between the data capture rates and the anticipated single bubble rising velocities in order to be able to apply cross-correlation techniques. Besides of driven guards, eight axial guard electrodes and eight finning guard electrodes are soldered and earthed along the axial and radial directions of the measuring electrodes. A piece of outer copper screen is attached and earthed to eliminate the effects of extraneous signals. Discharge resistors have been connected between each electrode and the outer screen to ensure that no static charge can build up on the electrodes and connecting leads to prevent potential damage on the capacitance measurement circuit.

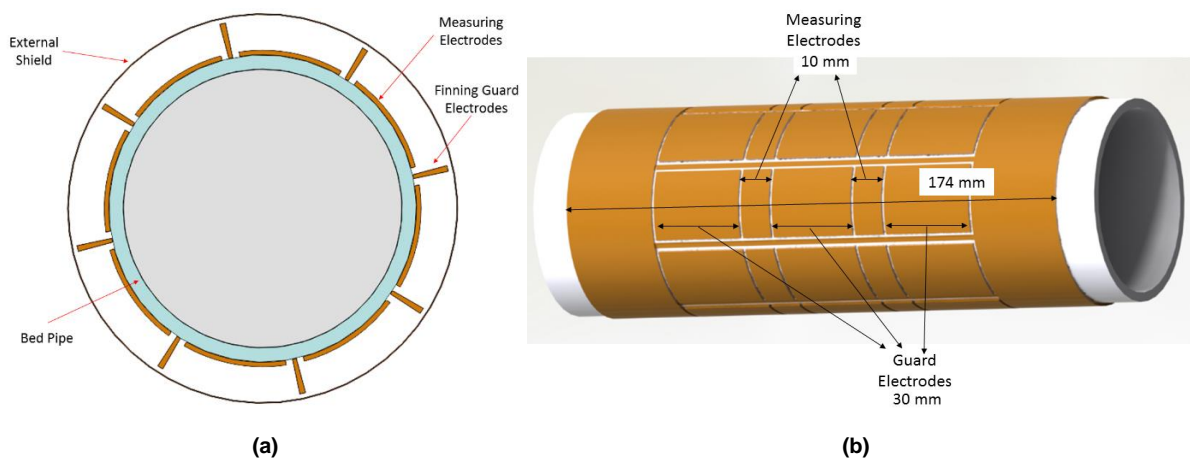


Figure 3. (a): 2D cross-sectional schematic diagram of ECT sensor; (b): 3D view and the dimensions for measuring electrodes and driven guard electrodes

3 CUT-OFF VALUE DETERMINATION

3.1 Experimental description for cut-off value determination

It has been known that a grey level denotes the reconstructed permittivity value for a specific pixel when the sensor is calibrated with high permittivity material (grey level is 1) and lower permittivity material (grey level is 0). As described in the introduction part, the bubble boundary value (the grey level cut-off value) has not been investigated systematically. In particular, some of the previous investigators used column phantoms to simply represent the spherical bubble shape, which may give distorted results as the bubble shapes have been found relating to spherical or hemispherical shape. In order to find the proposed 'realistic' bubble cut-off value, which can be used to estimate the bubble size in a single bubbling fluidized bed, five different plastic balls whose materials are polypropylene are used to have a systematic study. In order to move the plastic ball in a packed bed, an M3 screw with a pierced "cap" was tapped into the PVC air distributor to act as an anchor. A piece of fishing line goes through the plastic ball and is knotted on both sides to secure the ball to the fishing line. The ball can be dragged up and down along the pipe using the fishing line secured to the pierced screw cap at the distributor.. The details of the plastic balls are given below in Fig. 4 and Table 1.

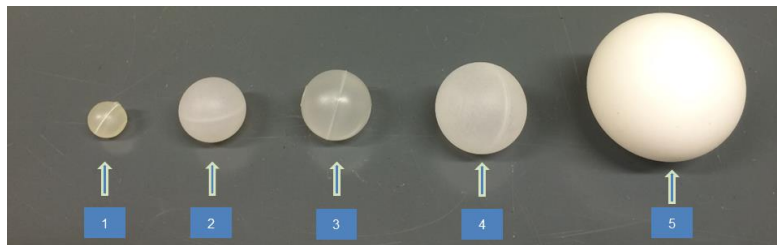


Figure 4. Images for five different plastic balls

From Table 1, it can be seen that the wall thickness is not negligible and moreover that it is not identical for all five balls. Theoretically, the differences of wall thickness may have influence on the measured capacitance value between each pair of the measuring electrodes. This may consequently affect the bubble boundary cut-off values. In order to examine whether the wall thickness will have a significant influence on the measured capacitance values, a three-dimensional numerical simulation was performed.

Table 1: Specifications of the five plastic balls

No.	Outer Diameter (mm)	Weight (g)	Wall Thickness(mm)	Internal Hollow Diameter (mm)	Internal cross section area (mm ²)
1	10	0.275	1.2	7.6	45.34
2	18.4	1.355	1.6	15.2	181.36
3	20	0.92	0.84	18.32	263.46
4	25.4	2.25	1.3	22.8	408.07
5	40	2.7	0.38	39.24	1208.72

3.2 Numerical simulation of ball wall effects

The AC/DC module in COMSOL Multiphysics (version 4.4) is utilized to simulate the electrostatic field and obtain the simulated capacitance values between each pair of measuring electrodes. A schematic drawing for the numerical simulation when a plastic ball is put inside of the packed bed is shown in Fig.5. The plastic ball theoretically is put symmetrically between the measuring electrodes. The primary purpose of the simulation is to check the differences when the wall material of the plastic ball is set as real polypropylene and the 'ideal' mixture of silica sand and air. The hollow area is

represented by the central white colour space, which is assumed as pure air (effective permittivity 1.0) in materials setting-up. The real effective permittivity of the plastic ball wall is 2.2. The material of the plastic pipe is acrylic whose effective permittivity is 2.7. The pseudo mixture effective permittivity of silica sand and air of the packed bed is derived by the following equation, the Maxwell Garnett Equation.

$$\left(\frac{\epsilon_{eff} - \epsilon_m}{\epsilon_{eff} + 2\epsilon_m}\right) = \delta_i \left(\frac{\epsilon_i - \epsilon_m}{\epsilon_i + 2\epsilon_m}\right) \quad (1)$$

where ϵ_{eff} is the effective dielectric constant of the medium, ϵ_i is the one of the inclusions (air), value=1; ϵ_m is the one of the matrix (silica sand), value=3.0; δ_i is the volume fraction of the inclusions, value=0.4. The resulting effective permittivity for the mixture of air and silica sand is 2.1.

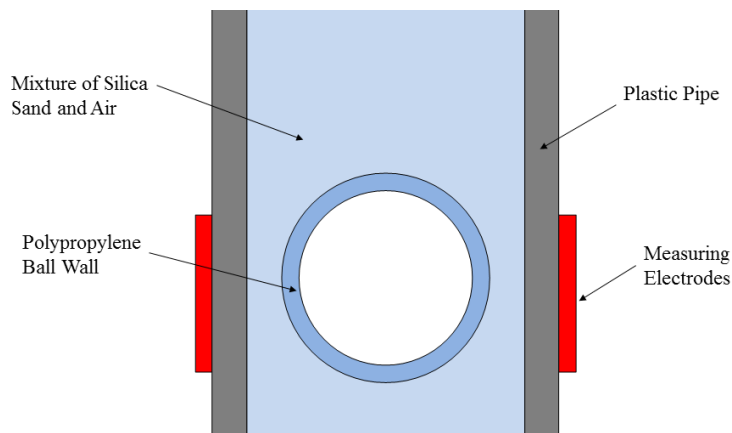


Figure 5. Schematic drawing for the numerical simulation when a plastic ball is put inside of the packed bed

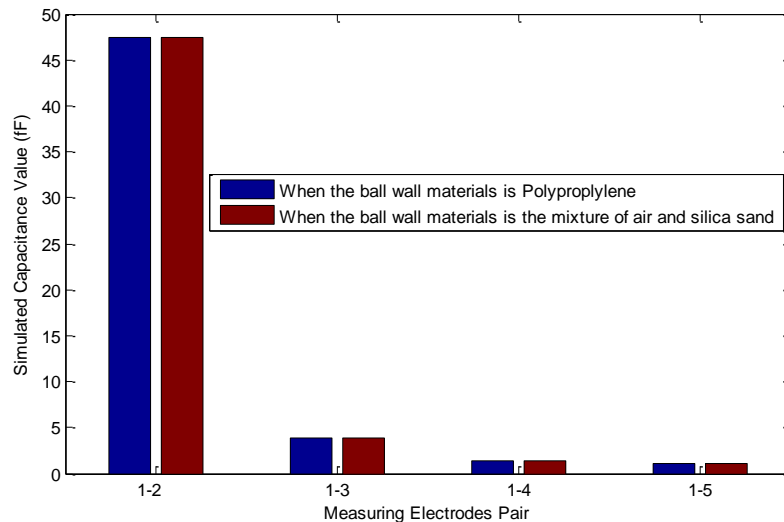


Figure 6. Simulated capacitance value for different measuring electrodes pair of the 40 mm outer diameter ball.

During the simulation process, the capacitance value is derived by the surface integral of the electrical charge density on the corresponding measuring electrodes pair area. A typical bar graph is provided in Fig.6 which shows the simulated results of the 40 mm outer diameter ball. In Fig. 6, only four pairs of measured capacitance value are displayed due to the symmetrical feature of the sensor. From Fig.6, under the above mentioned two conditions, the simulated capacitance is almost the same by observation (the actual largest percentage difference is 0.161% at Pair 1-4). According to the numerical simulation results for the five different balls, the largest percentage difference is around at

0.334%. This demonstrates that the plastic ball wall would have very limited effect on measured capacitance value, and that the hollow inside of the ball can be treated as a gas bubble surrounded by silica sand/air mixture.

3.3 Image reconstruction algorithm and permittivity model determination

It is well known that the simplest and most commonly used image reconstruction algorithm is the Linear Back Projection (LBP) method. It has the advantage of low computing demand and being less time-consuming in data processing. However, the images obtained by this kind of method have low quality in terms of accuracy. The Iterative LBP algorithm is an improved image reconstruction method. In this approach, LBP is used to calculate the set of normalized permittivities from the measured normalized capacitances (McKeen and Pugsley, 2002). The calculated permittivities are then used to back-calculate the capacitances to which these permittivities correspond. Then, the difference is taken between the original set of capacitance measurements and the back-calculated set of capacitances. The final image quality is improved during this iteration process. To investigate how many iterations are needed to extract reliable images, the iteration process is presented in Fig.7.

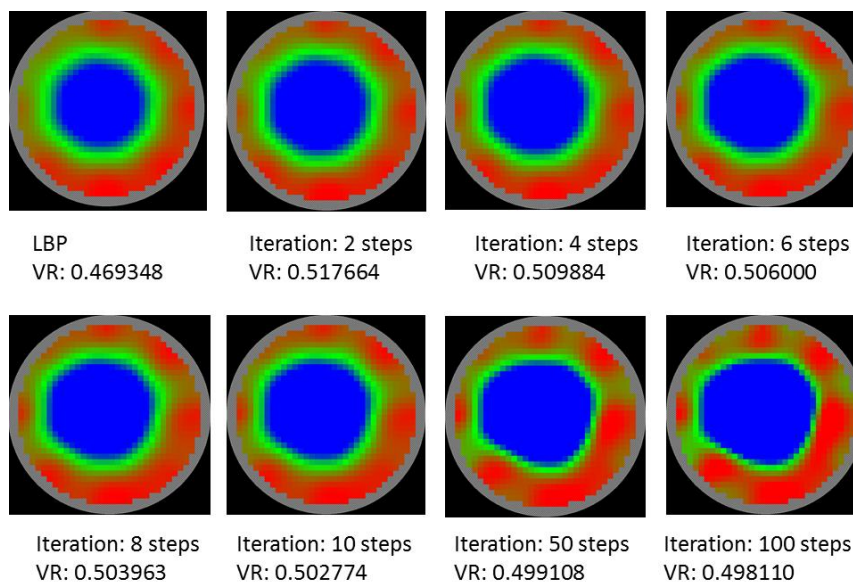


Figure 7. Iteration process using iterative LBP method with 40 mm plastic ball.

In Fig.7, a typical iterative process is implemented with the 40 mm plastic ball. The maximum iteration step applied is 100. VR stands for the overall volume ratio of the higher permittivity material (silica sand in this case). The overall volume ratio of the materials inside the sensor at any moment in time is defined to be the percentage of the volume of the sensor occupied by the higher permittivity material. The volume of the sensor is the product of the cross-sectional area of the sensor and the length of the sensor measurement electrodes. It can be found that with the increase of the number of iteration steps the volume ratio is reduced gradually which means the volume occupied by air is increased. The boundary of the air and silica sand becomes sharper. However, the iteration steps cannot be increased infinitely. The shape of the void is no longer circle-like after 50 iteration steps with a limited increment of VR. Therefore in this study, the images reconstructed by LBP and 10 steps of Iterative LBP methods will be analysed and compared. Also the parallel permittivity model will be used as it is regarded having the most accurate phantom test (McKeen and Pugsley, 2002).

Based on the aforementioned illustration, wall effect has very limited influence on capacitance values. Hence, the internal hollow area of the plastic balls can be treated as air phase solely. The basic procedures for extracting cut-off value distinguishing air and solid phases are as follows. A 32x32 pixel image is obtained when a plastic ball occupies the biggest area of the ECT sensor. The entire circular cross sectional area, whose equivalent diameter is regarded as the internal diameter (59 mm) of the fluidized bed pipe, has 812 effective pixels. According to the ratio of plastic ball hollow area to

fluidized bed pipe cross sectional area, the corresponding pixel number for the plastic ball hollow area can be calculated. The next step is to count the number of pixels starting from the lowest grey level until the cumulative number of pixels equals the pre-calculated number of pixels for the hollow area. The corresponding maximum grey level value is taken as the cut-off value for distinguishing solid and air phases. This procedure is repeated for all five balls. The cut-off values derived from the five plastic balls are summarised in Table 2. LBP and iterative LBP with 10 iteration steps (parallel permittivity model used in both cases) are used to extract cut-off values for the plastic balls.

Table 2: Cut-off value derived from five different plastic balls

Cut-off value derived from plastic balls						
No.	Outer Diameter (mm)	Internal Hollow Diameter (mm)	Near Centre		Near Wall	
			LBP	Iteration 10	LBP	Iteration 10
1	10	7.6	0.9394	0.9000	0.9200	0.9000
2	18.4	15.2	0.7700	0.7540	0.6999	0.6700
3	20	18.32	0.7687	0.7700	0.6646	0.6400
4	25.4	22.8	0.6300	0.6482	0.4948	0.4600
5	40	39.24	0.5835	0.5383	0.4441	0.4293

4 BUBBLE DIAMETER ESTIMATION FROM ECT MEASUREMENTS

With the extracted cut-off values for different plastic balls in Table 2, the equivalent diameter for a real bubble appearing in fluidized beds can be derived. Prior to determining bubble diameter, it is necessary to identify when a bubble occupies the most of the sensor volume. The sampling rate of ECT measurement is 200 frames per second (fps), which is sufficient to capture the bubble characteristics as the bubble frequency at bubbling flow regime in fluidized beds is normally less than 10 Hz. In Fig.8, a 5 second-long typical air volume ratio time series plot and its peaks are presented when superficial gas velocity is at 6.33 cm/s. The frames for which individual bubbles occupy the largest area of the pipe are identified by finding the local maxima in the volume ratio plot (see the circles in Fig. 8).

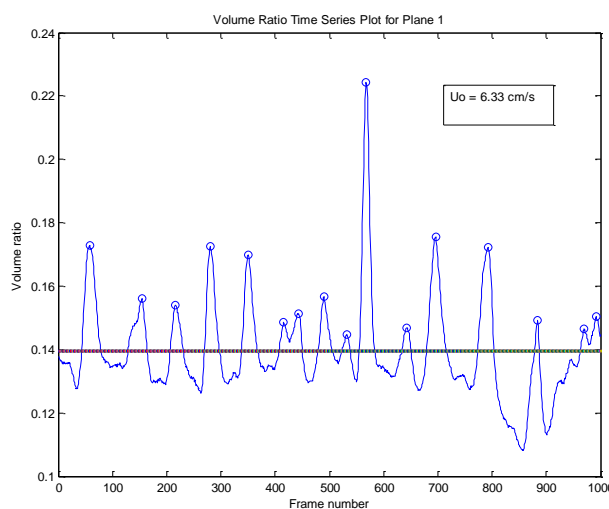


Figure 8. Volume ratio time series plot and its peaks when superficial velocity is at 6.33 cm/s.

As illustrated in Fig.9, the process of determining the bubble diameter is somewhat a 'reverse' of the process for deriving the cut-off values. It is acknowledged previously that there are 812 pixels for the

entire circular cross sectional area of the diameter of 59 mm (internal diameter of the fluidized bed pipe). Presuming an image for a bubble appearing in fluidized bed is acquired, sum up the number of pixels whose grey level values are below a cut-off value in Table 2 (there will be 20 counts available according to 20 cut-off values in the table). In accordance with the ratio of summed total pixel number for a real bubble to 812 pixels for the fluidized bed pipe cross sectional area, the corresponding equivalent diameter for a real bubble can be calculated (again there could be 20 bubble diameters calculated).

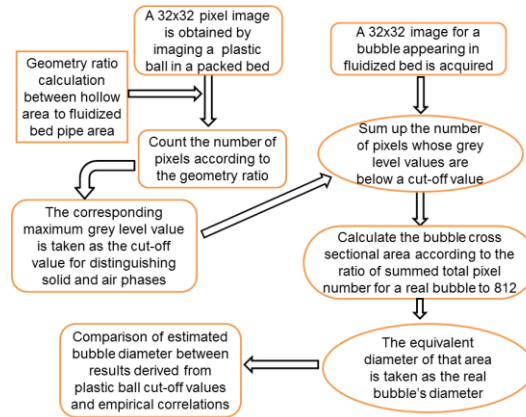


Figure 9. Flow chart for bubble diameter estimation process.

The calculated bubble diameter using the five different plastic ball cut-off values near centre and near wall derived by LBP method is shown in Fig. 10 and Fig. 11, respectively. In Fig. 10 and Fig. 11, the estimated bubble diameters are compared with five widely accepted correlations, i.e. Darton's equation, Rowe's equation, Werther's equation, Cai's equation and Mori's equation (Darton, 1977, Rowe, 1976, Werther, 1977, Cai et al., 1994, Mori and Wen, 1975). Similarly, Fig. 12 and Fig. 13 show the results derived from cut-off values near centre and near wall by 10-step iteration LBP method, respectively.

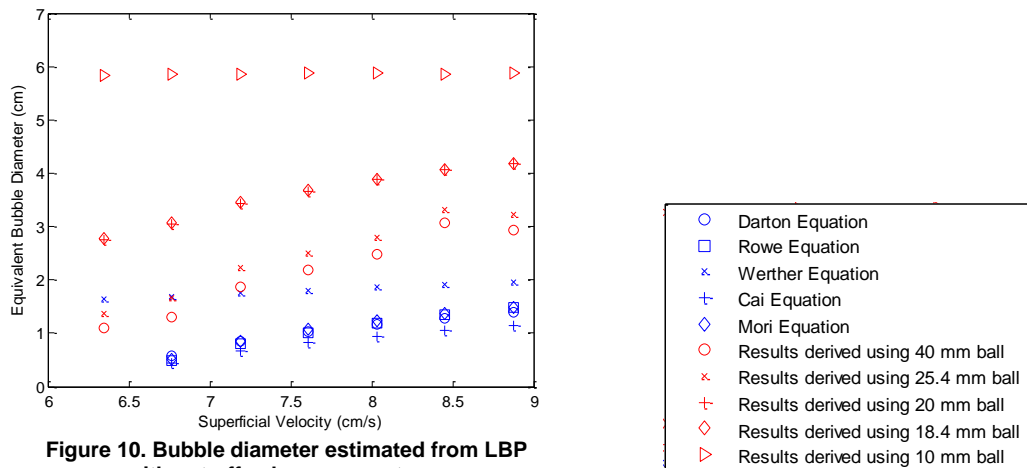


Figure 10. Bubble diameter estimated from LBP with cut-off value near centre.

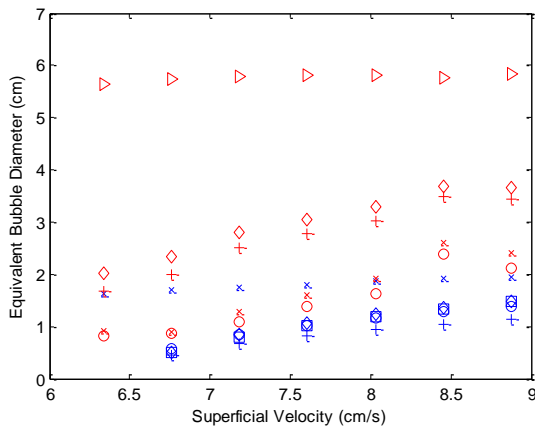


Figure 11. Bubble diameter estimated from LBP with cut-off value near wall.

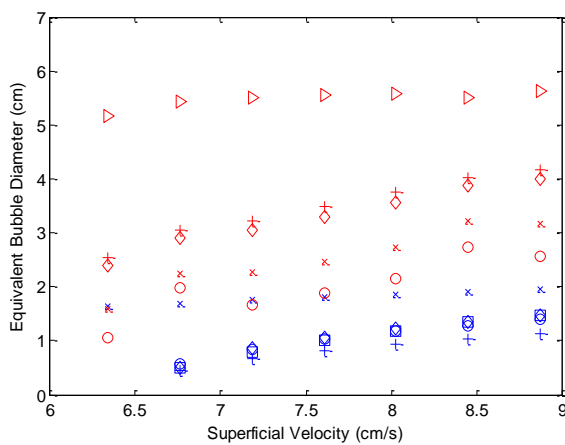


Figure 12. Bubble diameter estimated from 10 iteration LBP with cut-off value near centre.

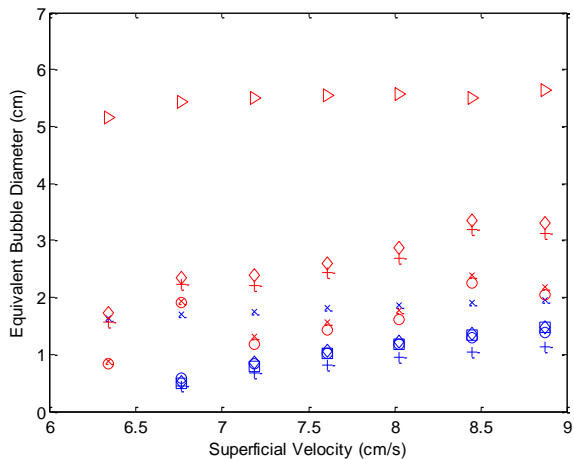


Figure 13. Bubble diameter estimated from 10 iteration LBP with cut-off value near wall.

- Darton Equation
- Rowe Equation
- × Werther Equation
- + Cai Equation
- ◇ Mori Equation
- Results derived using 40 mm ball
- × Results derived using 25.4 mm ball
- + Results derived using 20 mm ball
- ◇ Results derived using 18.4 mm ball
- ▽ Results derived using 10 mm ball

Firstly, by observing all four figures, five different empirical correlations give a good agreement between themselves, showing an increasing trend with the increasing superficial velocity. Furthermore, in Fig. 10 and Fig. 11, the bubble size estimated by cut-off value from 40 mm and 25.4 mm by LBP method near centre and near wall demonstrate obvious better consistency compared with the ones using 20 mm, 18.4 mm and 10 mm balls. In particular, the estimated bubble diameter is extremely distorted using cut-off value obtained from 10 mm balls. The main reason behind this phenomenon is largely attributed to that the internal hollow diameter of the 10 mm ball (7.6mm) is nearly the same level as the limited spatial resolution (tenth of the pipe diameter 5.9 mm).

Then, there are some clear discrepancies of the bubble diameter especially between estimated bubble diameter using 18.4 mm and 20 mm cut-off values and empirical correlations. This probably stems from the fact that the actual bubble size in the fluidized bed is already larger than 18.4 mm or 20 mm at higher superficial velocities (i.e. more than 7 cm/s from Fig.10 to Fig.13). At this stage, the cut-off values obtained from 18.4 mm and 20 mm plastic balls are possibly not suitable anymore (perhaps estimating larger bubble size demands cut-off values derived from larger plastic balls). Further investigation may be needed regarding this issue.

Moreover, the overall results obtained by using 40 mm cut-off values have the best agreement with Werther's equation result from Fig. 10 to Fig. 13. By looking at Fig. 12 and Fig. 13, the 10 iteration results show the 40 mm ball near centre cut-off value result has a good agreement before 7.5 cm/s while the corresponding results near wall cut-off value result exhibits better consistency after 7.5 cm/s. Nevertheless, results derived by 10 iteration overall display better similarity compared with empirical correlations than LBP algorithm.

5 CONCLUSIONS

Numerical simulation shows there would be very limited effect of plastic ball wall on simulated capacitance values. LBP and iterative LBP methods are used to extract the cut-off value of the five different plastic ball in a packed bed. The comparison between existing correlation results and estimated bubble diameter using 40 mm and 25.4 mm balls show good agreement. Overall, based on the plastic ball cut-off values, the estimated results by using 40 mm cut-off values show that Werther's equation has a better agreement compared with other four correlations. Results derived by 10 iteration LBP display a better similarity overall compared with empirical correlations than LBP algorithm. Current work is limited to the application for single bubbling flow regime. Future work will attempt to find how to extend this approach to turbulent flow regimes and seek how to apply varying cut-off values to the actual growing bubble diameter estimation. It will also aim to investigate the effect of different reconstruction algorithms and permittivity models on bubble size estimation to get more comprehensive understanding of bubble behaviour to examine the capability of ECT at estimating single bubble size within fluidized bed.

ACKNOWLEDGMENTS

The first author would like to thank the maintenance funding from China Scholarship Council and tuition fees funding from School of Civil Engineering, University of Leeds. Technician's supports from Mr Michael Marsden and Ms Susanne Patel are really appreciated. Useful advice on COMSOL simulation from Mr Yunjie Yang at University of Edinburgh is thanked.

REFERENCES

- CAI, P., SCHIAVETTI, M., DE MICHELE, G., GRAZZINI, G. & MICCIO, M. 1994. Quantitative estimation of bubble size in PFBC. *Powder technology*, 80, 99-109.
- CHANDRASEKERA, T., LI, Y., MOODY, D., SCHNELLMANN, M., DENNIS, J. & HOLLAND, D. 2015. Measurement of bubble sizes in fluidised beds using electrical capacitance tomography. *Chemical Engineering Science*, 126, 679-687.
- CHEREMISINOFF, N. P. 1986. Review of experimental methods for studying the hydrodynamics of gas-solid fluidized beds. *Industrial & Engineering Chemistry Process Design and Development*, 25, 329-351.
- DARTON, R. 1977. Bubble growth due to coalescence in fluidized beds. *Chem. Eng. Res. Des.*, 55, 274-280.
- DYAKOWSKI, T. & JAWORSKI, A. 2001. Application of non-invasive techniques for imaging fluidized beds—a review. *Handbook of Powder Technology*, 10, 807-823.
- DYAKOWSKI, T., JEANMEURE, L. F. & JAWORSKI, A. J. 2000. Applications of electrical tomography for gas–solids and liquid–solids flows—a review. *Powder technology*, 112, 174-192.

- HALOW, J. & NICOLETTI, P. 1992. Observations of fluidized bed coalescence using capacitance imaging. *Powder Technology*, 69, 255-277.
- KAGE, H., AGARI, M., OGURA, H. & MATSUNO, Y. 2000. Frequency analysis of pressure fluctuation in fluidized bed plenum and its confidence limit for detection of various modes of fluidization. *Advanced Powder Technology*, 11, 459-475.
- MCKEEN, T. R. & PUGSLEY, T. S. 2002. The influence of permittivity models on phantom images obtained from electrical capacitance tomography. *Measurement Science and technology*, 13, 1822.
- MORI, S. & WEN, C. 1975. Estimation of bubble diameter in gaseous fluidized beds. *AIChE Journal*, 21, 109-115.
- ROWE, P. N. 1976. Prediction of bubble size in a gas fluidised bed. *Chemical Engineering Science*, 31, 285-288.
- WANG, S. 1998. *Measurement of fluidization dynamics in fluidized beds using capacitance tomography*.
- WERTHER, J. 1977. Zur Problematik der masstabsvergroesserung von wirbelschichtreaktoren. *Chemie Ingenieur Technik*, 49, 777-785.